ADSORPTION OF TETRACHLOROALUMINATE ION ON GRAPHENE QUANTUM DOTS

Mr. Fadjar Mulya

จุฬาลงกรณ์มหาวิทยาลัย
CHULALONGKORN UNIVERSITY

A Thesis Submitted in Partial Fulfillment of the Requirements

for the Degree of Master of Science in Chemistry

Department of Chemistry

Faculty of Science

Chulalongkorn University

Academic Year 2018

การดูดซับไอออนเตตระคลอโรอะลูมิเนตบนแกรฟีนควอนตัมดอต

นายฟาด์จาร์ มุลยา

วิทยานิพนธ์นี้เป็นส่วนหนึ่งของการศึกษาตามหลักสูตรปริญญาวิทยาศาสตรมหาบัณฑิต
สาขาวิชาเคมี ภาควิชาเคมี
คณะวิทยาศาสตร์ จุฬาลงกรณ์มหาวิทยาลัย
ปีการศึกษา 2561
ลิขสิทธิ์ของจุฬาลงกรณ์มหาวิทยาลัย

Thesis Title	ADSORPTION OF TETRACHLOROALUMINATE ION ON GRAPHENE QUANTUM DOTS
By	Mr. Fadjar Mulya
Field of Study	Chemistry
Thesis Advisor	Associate Professor VUDHICHAI PARASUK, Ph.D.

Accepted by the Faculty of Science, Chulalongkorn University in Partial Fulfillment of the Requirement for the Master of Science

.... Dean of the Faculty of Science

(Professor POLKIT SANGVANICH, Ph.D.)

THESIS COMMITTEE

.... Chairman

(Assistant Professor VARAWUT TANGPASUTHADOL, Ph.D.)

.... Thesis Advisor

(Associate Professor VUDHICHAI PARASUK, Ph.D.)

.... Examiner

(Assistant Professor SAKULSUK UNARUNOTAI, Ph.D.)

.... External Examiner

(Chompoonut Rungnim, Ph.D.)

ฟาด์จาร์ มุลยา : การดูดซับไอออนเตตระคลอโรอะลูมิเนตบนแกรฟีนควอนตัมดอต. (ADSORPTION OF TETRACHLOROALUMINATE ION ON GRAPHENE QUANTUM DOTS) อ.ที่ปรึกษาหลัก : รศ. ดร.วุฒิชัย พาราสุข

สิ่งสำคัญในกลไกของแบตเตอรี่อลูมิเนียมไอออนคือการดูดซับที่รวดเร็วของเตเตระคลอโรอลูมิเนต [AlCl$_4$]$^-$ บนตำแหน่งแทรกของกราฟีนซึ่งสามารถเพิ่มประสิทธิภาพและอายุการใช้งานของแบตเตอรี่ ในการศึกษานี้เราใช้แกรฟีนควอนตัมดอต (GQDs) จำลองวัสดุแคโทด เพื่อที่จะศึกษาการดูดซับของ [AlCl$_4$]$^-$ บน GQDs โคโรนีน (coronene, C$_{24}$H$_{12}$) และเซอคัมโคโรนีน (circumcoronene, C$_{54}$H$_{18}$) เป็นแบบจำลองของแกรฟีนควอนตัมดอตโดยพิจารณาทั้งตำแหน่งการดูดซับและการจัดวางอย่างละสามรูปแบบ ประจุของ GQDs ปรับเป็น 0 และ +1 แทนสภาวะปล่อยและเก็บประจุและมีประจุ ระยะห่างระหว่างอะตอมคลอรีนกับอะตอมคาร์บอนบน GQDs พบว่ามีค่าอยู่ในช่วง 3.08-3.37 Å ตำแหน่งที่เสถียรที่สุดที่ [AlCl$_4$]$^-$ดูดซับบน GQDs คือ "H1" (ตำแหน่งฮอล์โลว์ที่กลางวง) ในสภาวะเก็บประจุ โดยมีค่าพลังงานดูดซับ -65.24 kcal/mol และระยะห่างระหว่างอะตอมคลอรีนกับอะตอมคาร์บอนเป็น 3.29 Å ค่าศักย์ไฟฟ้าของเซลล์ที่เกิดจากการดูดซับที่ตำแหน่งนี้คือ 3.66 V ดังนั้น GQDs จึงสามารถนำไปใช้เป็นวัสดุแคโทดสำหรับแบตเตอรี่อลูมิเนียมไอออนได้

สาขาวิชา	เคมี	ลายมือชื่อนิสิต ....
ปีการศึกษา	2561	ลายมือชื่อ อ.ที่ปรึกษาหลัก ....

6072085923 : MAJOR CHEMISTRY

KEYWORD: Battery, Aluminum, Adsorption, Graphene Quantum Dots

Fadjar Mulya : ADSORPTION OF TETRACHLOROALUMINATE ION ON GRAPHENE QUANTUM DOTS. Advisor: Assoc. Prof. VUDHICHAI PARASUK, Ph.D.

The important thing in the mechanism of aluminium ion battery is the fast adsorption of tetrachloroaluminate $[AlCl_4]^-$ on intercalation sites of bulk graphite which can increase the efficiency and lifetime of the battery. In this study, we modeled graphene quantum dots (GQDs) as cathode material. For the adsorption of $[AlCl_4]^-$, coronene ($C_{24}H_{12}$) and circumcoronene ($C_{54}H_{18}$) were used as the model of GQDs with three types of adsorption sites and standing positions. The charge of GQDs was modified to be 0 and +1 to address discharging and charging conditions. The distance between chlorine atom and carbon atom of GQDs was found to be between 3.08-3.37 Å. The most stable position for adsorption of $[AlCl_4]^-$ on GQDs is "H1" (hollow site at center of GQD) in the charging condition, with the adsorption energy of -65.24 kcal/mol, and the distance between chlorine atom and carbon atom is 3.29 Å. This adsorption corresponds to the cell potential of 3.66 V. GQDs can thus be recommended as a cathode material for aluminum ion battery.

จุฬาลงกรณ์มหาวิทยาลัย
CHULALONGKORN UNIVERSITY

Field of Study: Chemistry   Student's Signature ....
Academic Year: 2018   Advisor's Signature ....

ACKNOWLEDGEMENTS

TABLE OF CONTENTS

Page

LIST OF TABLES

LIST OF FIGURES

CHAPTER 1

INTRODUCTION

Nowadays, the demand for energy is growing up. The efficient and sustainable energy is highly necessary. One of alternative energy storages is metal-ion battery (MIB) which has several advantages such as concise size, high efficiency, and simple maintenance. In recent years, several MIB have been developed such as Lithium (Li), Sodium (Na), Magnesium (Mg), Zinc (Zn) and Aluminum (Al). Among them, Li ion battery is the most mature technology. However, it has several limitations such as costly productions and limited resources of lithium. To overcome the limitation of Li ion battery, researchers have developed other kinds of metal-ion batteries. One of the promising candidates is the aluminum ion battery since it has several advantages such as high abundance, high gravimetric density, low flammability, low reactivity, and the ability to exchange three electrons during electrochemical process [1-2].

However, the aluminum ion battery also has limitations such as cathode material disintegration, insufficient cycle life, low capacity, and low voltage. To solve these problems, many researchers have tried to find suitable cathode materials and electrolytes. One of the excellent reports was presented by Lin et.al [3] which employed aluminum metal as anode, carbon-based material (graphite) as cathode and $AlCl_3$ /[EMIm]Cl ionic liquid as electrolytes. Their report was a breakthrough to solving the limitation of the aluminum ion battery. Nonetheless, it still has important

questions to discuss such as the orientation of $AlCl_4^-$, preferred adsorption sites, and adsorption mechanism. The answers to these questions would help to improve the performance of the aluminum ion battery especially for the theoretical voltage. In this light, computational study can help us to understand the insight of the adsorption mechanism and predict the theoretical voltage of the aluminum ion battery. Furthermore, searching for alternative cathode materials will be an interesting topic to discuss. In this study, we propose graphene quantum dots for cathode materials to improve the performance of the aluminum ion battery.
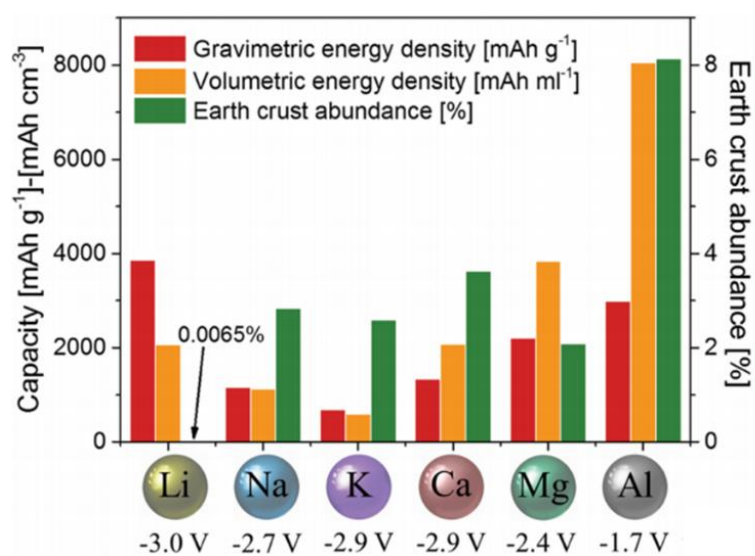
Figure 1.1. The comparison of metal-ion batteries.

1.1 LITERATURE REVIEW

➢ Aluminum Ion Battery

In review, Li and Bjerrum [4] explained how aluminum can be an anode material and classified the aluminum ion battery according to the used electrolytes, i.e. aqueous electrolyte primary batteries, aluminum-air batteries and molten salt secondary batteries. This review helped us to understand the aluminum ion battery which uses aluminum metal as anode for energy storage. They also proposed that aluminum batteries with molten salt have better performance than those with aqueous electrolyte because of several advantages such as high electrical conductivity, fast electrode kinetics, and high decomposition potential. Hence this battery is suitable to be developed as rechargeable aluminum batteries.

One of the limitations to develop rechargeable aluminum batteries is the cathode material disintegration. Transition metal oxide (TMO) is one of the choices for cathode materials because of the space for intercalation/de-intercalation during cycle life. Jayaprakash et al. [5] reported V_2O_5 nanowires as cathode and [EMIm]Cl as electrolyte for the rechargeable aluminium-ion battery. The battery delivered a discharge capacity of 305 mAh g^{-1} in the first cycle and 273 mAh g^{-1} after 20 cycles, with very stable electrochemical behavior. Nonetheless, the coulombic efficiency of the battery is poor. VO_2 nanorods which were considered to be highly reversible and stable cathode material for Lithium batteries were investigated by Wang et al. [6]. They used as-synthesized VO_2 nanorods as a cathode material with butyl-3-

methylimidazolium chloride ([BMIm]Cl) as an electrolyte and called super-valent battery. This battery has a long cycle life, low cost and good capacity. At the current density of 50 mAg^{-1}, the discharge capacity of the battery remains 116 $mAhg^{-1}$ after 100 cycles. TMOs (V_2O_5 and VO_2) are suggested as cathode materials for multivalent ion batteries owing to the variable valence and good stability transition metals. It increases the capacity, cycle life, and coulombic efficiency. Unlike monovalent lithium, trivalent Al batteries induced the strong coulombic effect which makes the electrochemical intercalation into a host crystal structure very challenging. Therefore, it still needs an improvement.

Another type of cathode material is carbon-based cathode materials. Owing to several advantages of carbon such as high conductivity, low cost, and abundance in nature. Porous carbon, activated carbon, graphitic carbon and amorphous carbon successfully improved the development of Lithium batteries. In developing rechargeable aluminum battery, Gifford and Palmisano [7] were the first researcher that used carbon-based cathode materials. They presented an Al/graphite battery using a room-temperature ionic liquid (RTIL) electrolyte. The average voltage is 1.7 V with discharge capacities in the range of 35 to 40 $mA\ hg^{-1}$ at current densities 1-10 $mA\ hg^{-1}$ and achieves more than 150 cycles. Nonetheless, it still has limitation about the evolution of Cl_2 gas. Sun et al. [8] introduced Al-ion battery with carbon paper as the cathode. The electrolyte is the mixture of $AlCl_3$:[EMIm]Cl. The high voltage plateau has been reported for this Al-ion battery. Even discharged at 100 $mA\ g^{-1}$, the

capacity can reach as high as 69.92 mA h g^{-1} over 100 cycles with high reversibility. Due to the low cost and abundance of raw materials (aluminium and graphite), the Al-ion battery established in this work showed the bright prospect for the commercial application. The important invention was done by Lin et al. [10]. They introduced the ultrafast rechargeable Al-ion battery which using graphitic foam as a cathode, aluminium as an anode, and ionic liquid electrolyte made from vacuum dried [EmIM]Cl. The proposed intercalation/de-intercalation of chloroaluminate anions in the graphite. They introduced a new Al-ion battery using novel graphitic cathode materials with a stable cycling life up to 7500 charge/discharge cycles without decay, very fast charging time of nearly 1 minute and extremely high current density of 4000 mA g^{-1}. This work contributed greatly to the development of rechargeable aluminum ion batteries. However, the battery only can afford an energy density ~40 W h kg^{-1} which is not suitable for high energy applications such as electric vehicles.

In most cases, the electrochemical performance of carbon-based cathode materials is mainly owing to intercalation/de-intercalation of monovalent chloroaluminate anions rather than trivalent Al^{3+} cations. The monovalent chemistry has achieved high capacity rechargeable aluminum ion batteries, To improve the capacity without reducing electrochemical performance, carbon-based materials which encourage trivalent reactions is highly requested.

Other types of cathode materials such as conducting polymer and Mo_6S_8 crystal have as well been reported. Hudak [9] used chloroaluminate-doped conducting polymers, polypyrrole, and polythiophene as cathode materials in a RTIL electrolyte. They reported discharge capacities between 30 and 100 mA h g^{-1}. Also, 100 % coulombic efficiency was attained for both polymer-based cathodes. Nonetheless, the dissolution of active materials into the electrolyte reduced the capacities. Furthermore, the average of low discharge voltages hindered the future development of conducting polymers-based cathodes. Geng et al. [10] demonstrated the reversible electrochemical Al intercalation when used Mo_6S_8 as the cathode material in a RTIL electrolyte for the first time. From the practical aspect, the theoretical material-level specific energy of a battery with Al anode and Mo_6S_8 cathode is approximately 90 W h kg^{-1} (assuming 0.5 V nominal voltage), which can be an attractive alternative for large-scale energy storage technologies.

Computational study also investigated the ultrafast rechargeable aluminum ion battery. Wu et al. [11] investigated $AlCl_4^-$ cluster intercalation and diffusion in graphite by using first principles calculations. Their results demonstrated the geometry of $AlCl_4$ cluster prefers to be planar plane than tetrahedral. Jung et al. [12] investigated the structure, ion conductivity, and mechanical property of $AlCl_4^-$-intercalated graphitic materials using first-principles calculation. Tetrahedral geometry, staging mechanism and the distance between C from graphene to Cl from

AlCl$_4^-$ was reported. Gao et al. [13] carried out first-principles calculations to provide a comprehensive understanding of the Al/graphite battery. They reported that the geometry of intercalant is tetrahedral, the distance between C from graphene to Cl from AlCl$_4^-$ should be greater than 3 Å, average voltage is 2.06 V, and preferable adsorption sites were hollow and on-top site. Bhauriyal [14] reported that aluminum ion battery has 4 staging mechanism during intercalation, tetrahedral is geometry, it has three preferable adsorption sites (bridge, hollow and on-top), average voltage is 2.01–2.3 V, and gravimetric capacities is 25.94 mA h g^{-1} and 69.62 mA h g^{-1}.

The recent issue to improve the performance of rechargeable batteries is graphene quantum dots (GQDs) as the cathode material. Because of several advantages such as high conductivity and large specific surface area, GQDs can be used as a nanostructured material for energy conversion and storage such as photovoltaic cells, supercapacitors, and rechargeable batteries [15-22]. GQDS consisting of two-dimensional graphene sheets with lateral dimension less than 100 nm in single, double or a few layers, have attracted tremendous attention owing to its remarkable electronic and physicochemical properties. Several studies also reported the adsorption mechanism of adsorbate on GQDs surface. To model the adsorption behavior in computational studies, the calculation must include the dispersion term [23-25].

➢ Graphene Quantum Dots (GQDs)

Zhu et al. [15] for the first time applied GQDs in surface engineering of lithium ion battery (LIB). They developed a novel CuO/Cu/GQD triaxial nanowires for the application in Li ion storage with higher capacities and improved rate and cycling stability than nanowires without GQDs. CuO/Cu/GQD triaxial nanowires showed high capacity retention in first 100 cycles and nearly no capacity decay afterward until 1000 cycles. Furthermore, the achieved high initial coulombic efficiency (ca. 87%) can be ascribed to a synergetic contribution from the Cu and GQD layers.

Chao et al. [16] invented high capacity, high rate, and durable lithium (Li) and sodium (Na) ion storage performance using GQDs coated onto the VO_2 surfaces. The GQDs layer brought further advantages in enhancing the electrochemical performance both in Li ion batteries and Na ion batteries. The integrated electrodes deliver the Na storage capacity of 306 mAh/g at 100mA/g, and the capacity of more than 110 mAh/g after 1500 cycles at 18 A/g. This result on Na-ion battery paves the way for the next generation of post-lithium (e.g., Na, Mg, and Al) batteries.

Guo et.al. [22] boosted the high-performance of Lithium-ion battery with doped GQDs into MoS_2 nanosheets. From their study, GQDs/ MoS_2 exhibits remarkably improved electrochemical lithium storages properties compared to pristine MoS_2, such as high reversible capacity (1099 mA h g^{-1} at 100 mA g^{-1}), good cyclic stability, as well as excellent rate performance (660 mA h g^{-1} at 5000 mA g^{-1}). Based on their result, they concluded that GQDs improve the electrical conductivity,

facilitate the charge transfer within the composite electrode, expanded the interlayer distance and promote Li^+ intercalation. Therefore, GQDs can be as well recommended as a cathode material of rechargeable aluminum batteries.

1.2 RESEARCH OBJECTIVES

In this study, two models of hexagonal-shape GQDs cathode materials were investigated. Preferable standing positions of $AlCl_4^-$, and adsorption sites, charge distribution, adsorption energy, and the theoretical voltage were answered in this study.
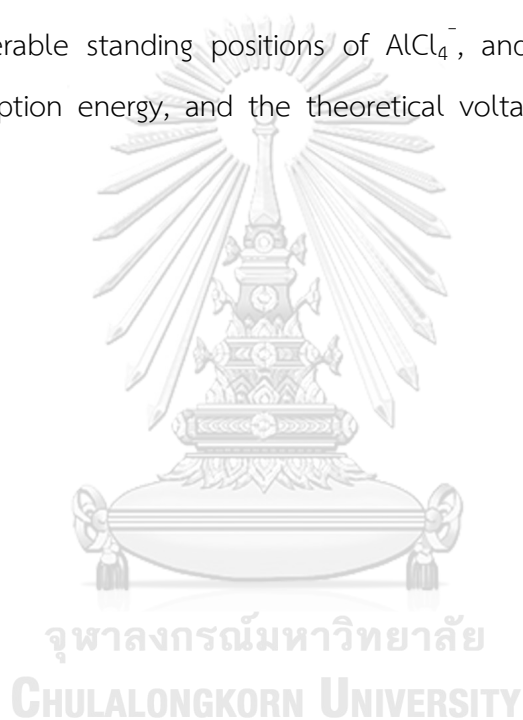
CHAPTER 2

THEORETICAL BACKGROUND

2.1 QUANTUM CHEMISTRY

To study microscopic level, it is unwise to use classical mechanics which can only describe macroscopic level. A new form of mechanics, called quantum mechanics is required. Quantum chemistry was formulated by laws of physics which applied quantum mechanics to solve the problems in chemistry. To describe the movements and interaction between electron and nuclei, Schrödinger equation is the principal formula in quantum chemistry. In quantum chemical calculations, there are two methods which have been used to elucidate electronic and molecular properties, wave-function based and density-based (density functional theory) methods.

2.1.1 The Schrödinger Equation

There are two forms for the Schrödinger equation, the time-dependent and time-independent Schrödinger equation. In the time-dependent Schrödinger equation, the wavefunction depends on time (equation 2.1), while in time-independent Schrödinger equation, it forms stationary states or standing waves (equation 2.2).

$$\hat{H}\,\Psi(x,t) = i\hbar\frac{\partial}{\partial t}\Psi(x,t) \qquad (2.1)$$

$$\hat{H}\,\Psi = E\Psi \qquad (2.2)$$

Where $\hat{H}$ is the Hamiltonian operator, Ψ is the wavefunction, E is the energy of the state, i is the imaginary unit, and $\hbar$ is the planck's constant divided by 2π. The Hamiltonian operator for the molecular system consists of nuclear kinetic term, electron kinetic term, electron-nuclear attraction term, electron-electron repulsion term, and nuclear-nuclear repulsion term [26].

$$H = T_N + T_E + V_{NE} + V_{EE} + V_{NN} \qquad (2.3)$$

where $\quad T_N$ = nuclear kinetic term,

$$= \sum_A -\frac{1}{2M_A}\nabla^2_A$$

T_e = electron kinetic term,

$$= \sum_i -\frac{1}{2}\nabla^2_i$$

V_{Ne} = electron-nuclear attraction term,

$$= \sum_A \sum_i -\frac{Z_A}{|\vec{R}_A - \vec{r}_j|}$$

V_{ee} = electron-electron repulsion term,

$$= \sum_{i<j} |\vec{r}_i - \vec{r}_j|^{-1}$$

and $\quad V_{NN}$ = nuclear-nuclear repulsion term.

$$= \sum_{A<B} \frac{Z_A Z_B}{|\vec{R}_A - \vec{R}_B|}$$

The equation (2.3) involves 3N nuclear coordinates and 3N electron coordinates. To reduce the complexity of the equation, Born and Oppenheimer [27] introduced an approximation based on the fact that electrons move much faster than nuclei due to

their mass. Hence, the problem is reduced by solving the electronic Schrödinger equation.

$$\psi\left(\vec{r},\vec{R}\right) = \chi_{nuc}\left(\vec{R}\right)\psi_{elec}\left(\vec{r};\vec{R}\right)$$

$$H_{elec} = T_E + V_{NE} + V_{EE} \tag{2.4}$$

$$\text{and } H_{elec}\,\psi_{elec}\left(\vec{r};\vec{R}\right) = E_{elec}\,\psi_{elec}\left(\vec{r};\vec{R}\right) \tag{2.5}$$

$\chi_{nuc}\left(\vec{R}\right)$ is the nuclear wavefunction. $\Psi_{elec}(\vec{r};\vec{R})$ is the electronic wavefunction which is the function of electron coordinates and parametrically depends on nuclei position $\vec{R}$. E_{elec} is electronic energy and the total energy E_{total} is

$$E_{total} = E_{elec} + V_{NN} \tag{2.6}$$

2.1.2 Hartree-Fock (HF) Approximation

Because of the electron-electron repulsion term, it is impossible to get the exact solution for (equation 2.5). To circumvent this, HF approximation uses the meant field approach for the electron-electron repulsion. The mean field approach is widely used in solid state and statistical physics [28-29]. The energy of an approximate wave function can be calculated as the expectation value of the Hamiltonian operator, divided by the norm of the wave function:

$$E_e = \frac{<\Psi\,|\,H_e\,|\,\Psi>}{<\Psi\,|\,\Psi>} \tag{2.7}$$

For a normalized wave function the denominator is 1, and therefore

$$E_e = <\Psi\,|\,H_e\,|\,\Psi> \tag{2.8}$$

Because of Pauli principle, the state required antisymmetric wave-function which can be achieved by building it from Slater Determinants.

$$|\psi_0(\vec{x}_1, \vec{x}_2, \ldots \vec{x}_N)\rangle = \frac{1}{\sqrt{N!}} \begin{vmatrix} \chi_1(\vec{x}_1)\chi_2(\vec{x}_1)\cdots\chi_N(\vec{x}_1) \\ \chi_1(\vec{x}_2)\chi_2(\vec{x}_2)\cdots\chi_N(\vec{x}_2) \\ \vdots \\ \chi_1(\vec{x}_N)\chi_2(\vec{x}_N)\cdots\chi_N(\vec{x}_N) \end{vmatrix} \qquad (2.9)$$

where $\chi_j(\vec{x}_i)$ = molecular (spin) orbital = $\chi_j(\vec{r}_i, \vec{\omega}_i)$,

$\vec{x}_i$ = spatial-spin coordinate,

$\vec{r}_i$ = spatial coordinate,

and $\vec{\omega}_i$ = spin coordinate.

$\chi_j(\vec{x}_i)$ can be acquired from the Fock equation

$$\hat{f}\chi_i = \varepsilon_i\chi_i \quad , \text{i=1, 2, ..., N} \qquad (2.10)$$

where, $\hat{f}$ is the Fock Operator and ε_i is the orbital energy.

In which

$$\hat{f} = -\frac{1}{2}\nabla_i^2 - \sum_{A_{el}}^{N}\frac{Z_A}{r_{iA}} + V_{HF}(i) \qquad (2.11)$$

where $V_{HF}(i)$ = mean field potential

With introducing basis function, we can determine as

$$\mathbb{F}\mathbb{C} = \mathbb{S}\mathbb{C}\mathbb{E} \qquad (2.12)$$

where $\mathbb{F}$ = Fock matrix,

$\mathbb{C}$ = Molecular orbital coefficients matrix,

$\mathbb{S}$ = Overlap matrix

and $\qquad$ $\mathbb{E}$ = Matrix of orbital energies

The equation is also called "Roothan-Hall" [30-31] equation. In terms of molecular orbital, the Hartree-Fock energy is

$$E_{HF} = \sum_a \left[\overset{x}{a} \mid -\frac{1}{2}\nabla_i^2 - \sum_A \frac{z_A}{\mid R_A - r_i \mid} \mid a \right] + \frac{1}{2}\sum_a \overset{x}{\sum_b}\left[aa \mid bb\right] - \left[ab \mid ba\right] \qquad (2.13)$$

The first term is one-electron integral and the second term is two electron integral, Coulomb and Exchange integral, respectively. The choice of basis set affected very much to achieve the convergence and the accuracy of HF.

2.1.3 Density Functional Theory

The lack of electron correlation is the problem of density functional theory (DFT). HF and all electron correlation methods are based on wavefunction which gives rise to the four-centered two-electron integrals. DFT method is based on Hohenberg-Kohn and Kohn-Sham equation [32]. The approximation of exchange correlation function of DFT much affects to the accuracy of calculation [33-34].

Hohenberg-Kohn postulated that the energy and properties of the ground state electron density (ρ) of the system can be determined from the function of position: $\rho = \rho(x, y, \text{z})$.

In terms of density, the electronic energy can be determined by:

$$E[\rho] = T[\rho] + V_{ext}[\rho] + V_{ee}[\rho] \qquad (2.14)$$

In which

$$J[\rho] = \frac{1}{2} \int \int \frac{\rho(r_1)\rho(r_2)}{\Delta r_{12}} dr_1 dr_2 \tag{2.15}$$

where $T[\rho]$ is the kinetic energy, $V_{ext}[\rho]$ is the kinetic energy of the external potential $V_{ee}[\rho]$ is two-electron interaction, while $J[\rho]$ is the Coulombic interaction. Hohenberg-Kohn proved that the density is uniquely determined for a particular-molecular system and the trial density can be used to obtain DFT energy via variation principle.

Kohn-Sham proposed the trial density which constructed by Kohn-Sham orbital (φ_i).

Therefore,
$$\rho(\vec{r}) = \sum_i |\varphi_i(\vec{r})|^2 \tag{2.16}$$

Most DFT applications are based on Kohn-Sham formula, in which

$$\left[-\frac{\nabla^2}{2} + V_s(r) \right] \varphi_i(r) = \varepsilon_i \varphi_i(r) \tag{2.17}$$

where $V_s(r)$ = Kohn-Sham potential

$$= \sum_A \frac{Z_A}{|R_A - r_i|} + \int \frac{\rho(r)}{|r - r'|} dr' + \frac{\partial E_{xc}[\rho]}{\partial p(r)} \tag{2.18}$$

and ε_i = Kohn-Sham orbital energy.

Kohn-Sham proposed

$$E[\rho] = T_s[\rho] + V_{ext}[\rho] + J[P] + E_{XC}[\rho] \tag{2.19}$$

The $E_{xc}[\rho]$ is the exchange-correlation function and equal to

$$E_{xc}[\rho] = T[\rho] - T_s[\rho] + V_{ee}[\rho] - J[P]$$

Where : $\mathbf{T}[\rho]$ is the kinetic energy, $\mathbf{T}_s[\rho]$ kinetic energy of non-interacting system,

$V_{ee}[\rho]$ is two-electron interaction, and $J[P]$ is the Coulombic interaction.

➢ Exchange-correlation functional

Based on the development, exchange-correlation functional in DFT can be classified in to 4 functionals.

1. Local density approximation (LDA). The functional depends only on the local density at a given point. Example: S-VWN

2. Gradient-corrected approximation (GGA): The functional depends on local density and its gradient. Examples: PW91 and LYP correlation functionals, B88 exchange functional

3. Meta-GGA: The Functional depends on density, its gradient, and its second derivative. Example: M06-L

4. Hybrid DFT: The Functional mixes in Hartree-Fock exchange. Most popular example: B3LYP (hybrid GGA). M05-2X and M06-2X are hybrid meta-GGA's.

2.1.4 Basis Set

Basis set is a set of known mathematical function. It affected the accuracy of quantum chemical calculations. The two types of renowned basis set are Slater type orbital (STO) [35] and Gaussian type orbital (GTO) [36]. Slater type atomic orbital emulates the solution of the Schrodinger equation for H atom, Therefore,

$$\phi^{STO}(\mathrm{r},\theta,\phi) = \mathrm{R}_{nl}^{STO}(r)Y_{lm}(\theta,\phi) \qquad (2.20)$$

where $\mathbf{R}_{nl}^{STO}$ = radial part of wavefunction

$$= \frac{(2\xi)^{\frac{3}{2}}}{\sqrt{(2l+2)}}(2\xi)^{l_1}e^{-\xi r} \tag{2.21}$$

and $Y_{lm}(\theta,\phi)$ = spherical harmonic function

Nevertheless, the exchange integral is impossible to solve analytically using STO functions and it is time consuming to compute numerically. Gaussian type atomic orbital described by

$$\phi = Nx^a y^b z^c e^{-\alpha r^2} \tag{2.22}$$

where x, y, and z are Cartessian coordinates and a, b, and c are non-negative integers. The advantage of GTO is the evaluation of two-eletron integrals which can be done without numerical integration.

➢ **Type of basis sets**

Basis set can be classified as a minimal basis set and extended basis set. In minimal basis set, numbers of basic function are the same as numbers of occupied orbitals in atom. The most popular minimal basis set is STO-nG, where n represents the number of primitive Gaussian functions which contains one basis function. The advantage of this basis set is it imitate STO. Disadvantage, it can not describe chemical bond very well. The general minimal-basis set are: STO-3G, STO-4G etc. [37]. Using multiple functions is the solution to solve the accuracy of minimal basis set. This is the concept for extended basis set. One way to construct the extended basis-set is the addition of more valence orbitals, so called split-valence basis set.

○   Split-valence basis sets

Separated between core and valence electrons. Core orbitals continue to be represented by a single (contracted) basis function, while valence orbitals can be split into arbitrarily many functions. Develop to solve the problem of inadequate description of anisotropic electron distributions using minimal basis sets. The most renowned split-valence basis set is X-YZG where X represents the number of primitive Gaussians comprising each core atomic orbital basis function, Y and Z represents the valence orbitals are composed of two basis functions, the first is a linear combination of Y primitive Gaussian functions, the other are the linear combination of Z primitive Gaussian functions such as 3-21 G, 6-31 G etc.

○   Polarized basis sets

In polarized basis sets, orbitals with higher angular momentum functions are added to appropriately describing the chemical bonding. Hydrogen atom in a minimal basis set would have one 1s atomic orbital. Adding a p-function to the basis set of hydrogen atom would the orbital to polarize and form sigma bond. In X-YZG basis set star or double star are added to the notation to signify polarized basis set. For example, 6-31G* or 6-31G(d) represents polarized function d on heavy atom, and 6-31G** or 6-31G(d,p) represents polarized function d on heavy atom and p on H atom.

2.2 THE BASIC PRINCIPLE OF RECHARGEABLE ALUMINUM ION BATTERY

The rechargeable aluminum-ion battery which employed aluminum metal as the anode, $AlCl_3$:[EMIM]Cl (1.3:1 mole ratio) as the electrolyte and a carbon based cathode shows a remarkable performance. The electrochemical process involves the dissolution of Al from the anode with the formation of $AlCl_4^-$ and $Al_2Cl_7^-$ species, and the intercalation of $AlCl_4^-$ in the cathode as shown in figure 2.1. [3].
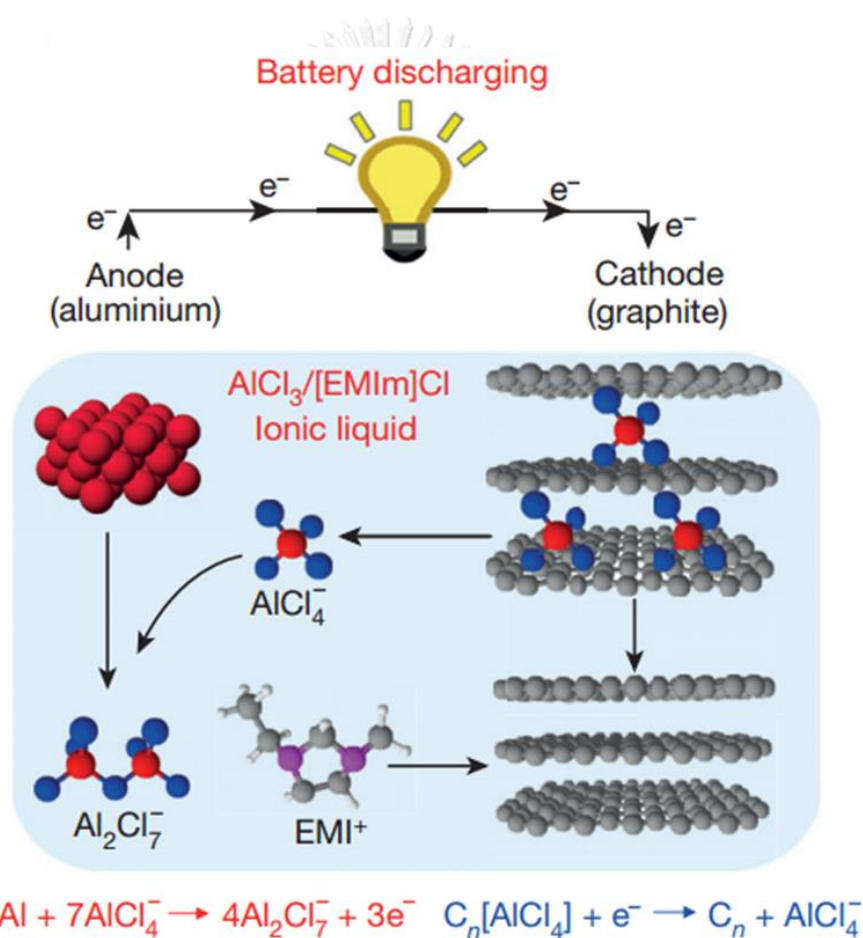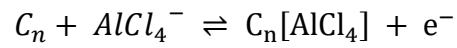

Figure 2.1. Schematic drawing of the Al/ graphite cell during discharging, using the optimal composition of the AlCl₃ /[EMIm]Cl ionic liquid electrolyte. The reverse reaction took place during charging.

The simplified Al/graphite cell redox reactions can be written as:

$$4Al_2Cl_7^- + 3e^- \rightleftharpoons Al + 7AlCl_4^-$$

$$C_n + AlCl_4^- \rightleftharpoons C_n[AlCl_4] + e^-$$
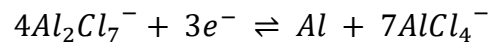
where n is the molar ratio of carbon atoms to intercalated anions in the graphite.

The $AlCl_4^-$ and $Al_2Cl_7^-$ concentrations in the electrolyte allowed for an optimal charging capacity at the cathode, with the abundant $AlCl_4^-$ for charging/intercalation in graphite and sufficient $Al_2Cl_7^-$ concentration for charging/electrodeposition at the anode.

CHAPTER 3

DETAILS OF THE CALCULATION

3.1 COMPUTATIONAL DETAILS

Coronene ($C_{24}H_{12}$) and circumcoronene ($C_{54}H_{18}$) were used as models of hexagonal-shaped GQDs cathode materials, as shown in Fig. 3.1. Three possible adsorption sites of $[AlCl_4]^-$, i.e. bridge (b), hollow (h), and on-top (t), were considered on GQDs with three types of $[AlCl_4]^-$ standing positions, as given in Fig. 3.2. Also, the pattern of adsorption sites based on zone of GQDs shown in Fig. 3.3.

All calculations were performed based on the density functional theory (DFT) method, with M06-2X hybrid functional [39] and 6-31G+(d) basis set using Gaussian09 software program. The charge of GQDs was designed to be q=0 and q=+1 to mimic discharging and charging conditions, respectively. The adsorption energy (E_{ad}) of adsorbate and GQDs was calculated by:

$$E_{ad} = E_{[AlCl_4]GQDs} - E_{AlCl_4} - E_{GQDs} \qquad (3.1)$$

where E_{ad} is the adsorption energy, $E_{[AlCl_4]GQDs}$ is the total energy of the adsorption complex, E_{AlCl_4} is the total energy of the molecular adsorbate ($[AlCl_4]^-$), and E_{GQDs} is the total energy of GQDs.

Theoretical voltage of [AlCl₄]-coronene and [AlCl₄]-circumcoronene can be obtained by:

$$V = \frac{-\Delta E}{nF} \qquad (3.2)$$

Where n is the number of transferring electrons, F is the faraday constant and ΔE is the cell potential.

3.2 RESEARCH PROCEDURE

Firstly, structures of $[AlCl_4]^-$ and $C_{24}H_{12}$, and $C_{24}H_{12}$-$[AlCl_4]^-$ with various charge schemes and spin multiplicities were optimized. Secondly, adsorption energies according to equation (3.1) were determined. From this result, preferable adsorption sites on GQDs surface and standing positions of $[AlCl_4]^-$ were obtained. Thirdly, calculations on larger GQDs such as $C_{54}H_{18}$ was additionally carried out. Again, preferable GQDs-$[AlCl_4]^-$ adsorption sites and standing positions of $[AlCl_4]^-$ were resulted. Finally, Analysis on distances between chlorine atom in $[AlCl_4]^-$ and GQDs, atomic charge distribution, and electrostatic potential were then made.
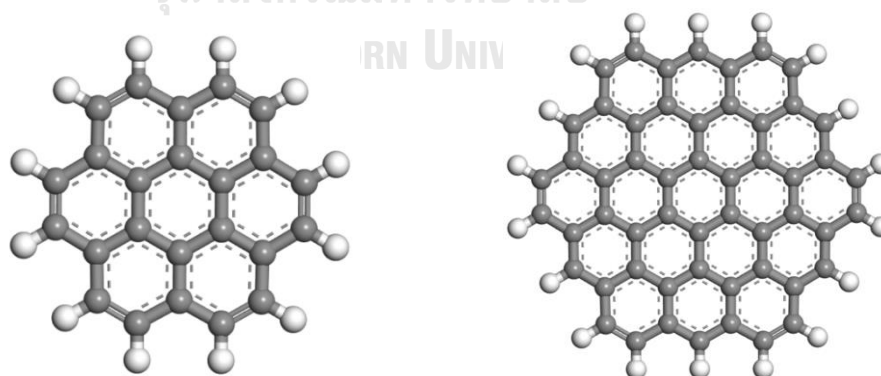
Figure 3.1. Schematic of the hexagonal-shape GQDs cluster models ($C_{24}H_{12}$ and $C_{54}H_{18}$).

bridge (B)   hollow (H)   on-top (T)

I   II   III
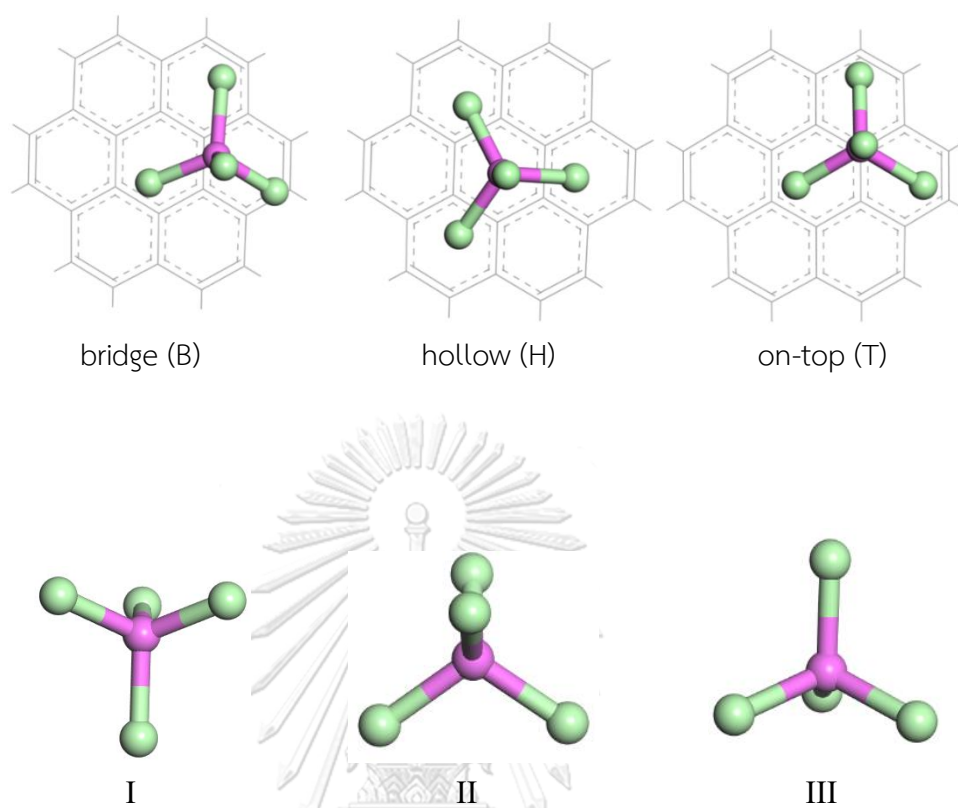
Figure 3.2. Schematic of the adsorption sites and standing position of $[AlCl_4]^-$.

Figure 3.3. The pattern of adsorption sites GQDs, classified based on the area of GQDs: central area (aqua), intermediate area (green) and edge area (yellow).

Areas of GQDs can be classified into central, intermediate, and edge as proposed by Lanza [40]. This classification helped us to reduce the number the calculations for predicting GQDs structure and properties.

CHAPTER 4

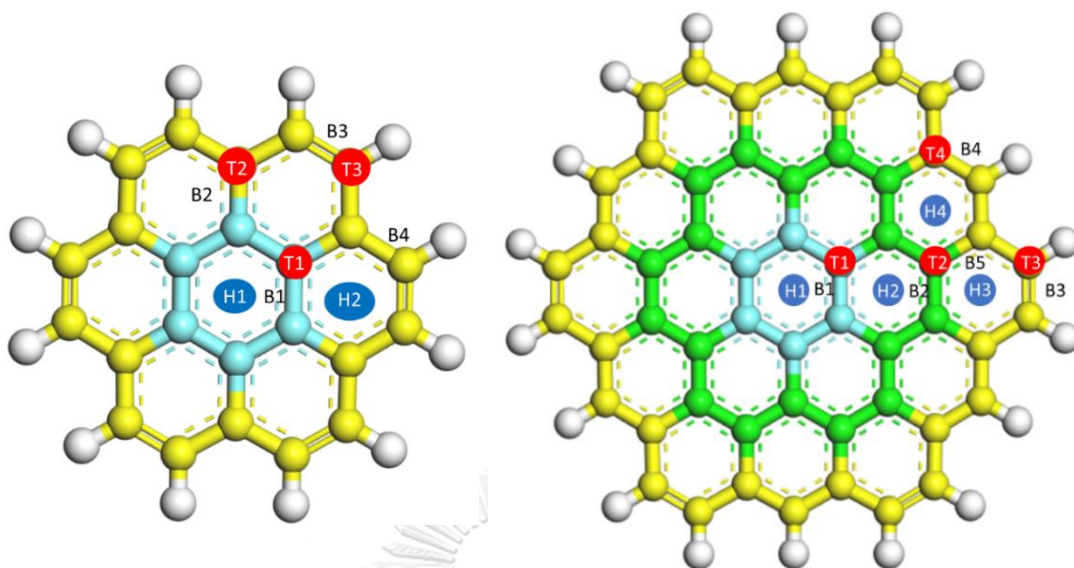RESULT AND DISCUSSION

4.1 ADSORPTION ON CORONENE

All possible patterns of adsorption site and standing position on coronene were examined. In addition, conditions of discharging and charging were considered. After geometry optimization for [AlCl$_4$]-coronene complexes, we classified into two categories, bind and unbind, as given in Table 4.1. In addition, for the bind structures starting geometries might change after optimization. Adsorption positions were designated as hollow (H), bridge (B) and on-top (T) as given in Figure 3.3. For each adsorption position, three standing positions, I, II, and III as described in chapter III were considered. The standing position III was found for most bind adsorptions. For the charging condition, only the standing position III was observed. For the discharging condition, we obtained a large number of unbind results.
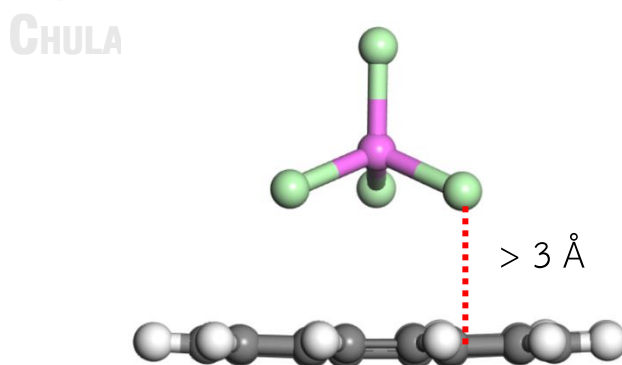

Figure 4.1. The structure of [AlCl$_4$]-corone on side view

Table 4.1. Optimized structures of [AlCl$_4$]-coronene

in discharging and charging condition

Sites and Standing	After optimization on discharging condition			After optimization on charging condition		
	I	II	III	I	II	III
B1	Unbind	T2-III	T1-III	B2-III	B1-III	H1-III
B2	Unbind	T2-III	T2-III	H1-III	H1-III	B2-III
B3	Unbind	Unbind	Unbind	H1-III	T3-III	T3-III
B4	Unbind	Unbind	B4-III	H1-III	B4-III	B2-III
H1	H1-I	H1-II	H1-III	T3-III	B2-III	H1-III
H2	Unbind	H2-II	T2-III	H1-III	H1-III	H1-III
T1	Unbind	B4-III	T1-III	B4-III	B1-III	H1-III
T2	Unbind	Unbind	T2-III	H1-III	T1-III	B2-III
T3	Unbind	Unbind	Unbind	H1-III	T3-III	T3-III

4.1.1 Charging Condition

For charging condition, the cathode reaction is $C_n + AlCl_4^- \rightarrow Cn[AlCl_4] + e^-$.

To maintain the charge equality for both orde of reaction, $Cn[AlCl_4]$ must be

neutral. Since $[AlCl_4]^-$ charge is -1, The C$_n$ charge is +1. Therefore, the coronene

charge is set to +1 to mimic the charging condition.

4.1.1.1 Adsorption energy in charging condition

Adsorption energies of $AlCl_4$ on coronene were calculated using equation (3.1). We obtained large negative adsorption energies for all bind adsorptions in Table 4.1. The negative adsorption energy indicates that the adsorption of $[AlCl_4]^-$ on coronene is favorable (exothermic). Adsorption energies of $[AlCl_4]^-$ on coronene in charging condition were listed in Table 4.2.

Adsorption energies between -63.03 to –65.24 kcal/mol were observed. The strongest adsorption is noticed for H1-III with the adsorption energy of -65.24 kcal/mol. As mentioned in the previous section, standing position III is the only preference position for the charging case. In the standing position III, three negatively charge chlorine atoms point downward to the positively charged surface. This position shows the strongest coulombic interaction and becomes the most favorite standing position. Thus, the interaction between $[AlCl_4]^-$ and the surface is very strong in charging condition.
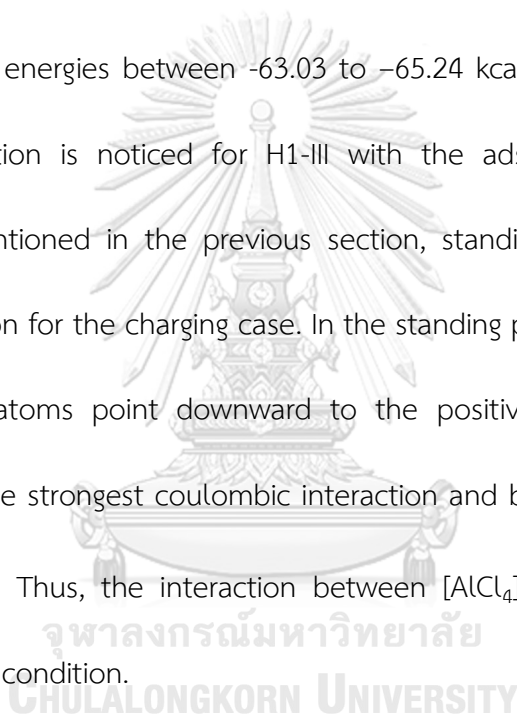
Table 4.2. Possible adsorptions, adsorption energies, voltage and
Mulliken charges of [AlCl$_4$]-coronene in charging condition

Adsorption Pattern	E$_{ads}$ (kcal/mol)	C-Cl distance	Mulliken Charge of AlCl$_4^-$	Mulliken Charge of GQDs
H1-III	-65.24	3.29	-0.84	0.84
B1-III	-64.08	3.31	-0.83	0.83
B2-III	-64.07	3.29	-0.82	0.82
B4-III	-63.20	3.12	-0.81	0.81
T1-III	-64.05	3.33	-0.82	0.82
T3-III	-63.03	3.09	-0.80	0.80

4.1.1.2 Charge transfer in charging condition

To understand the interaction between [AlCl$_4$]$^-$ and coronene surface, we evaluated the charge of [AlCl$_4$]$^-$ after adsorption. The molecular charge of [AlCl$_4$]$^-$ before the adsorption is -1. Net charges of [AlCl$_4$]$^-$ after adsorption on coronene surface in charging condition and various adsorption patterns were shown in Table 4.2. The charges are in the range of -0.80 to -0.84. These values are higher than the [AlCl$_4$]$^-$ molecular charge. Therefore, there is the charge transfer from [AlCl$_4$]$^-$ to coronene surface. This can also be viewed from electrostatic potential map in Figure 4.2. From the figure, it is noted that coronene become less positive after the adsorption.
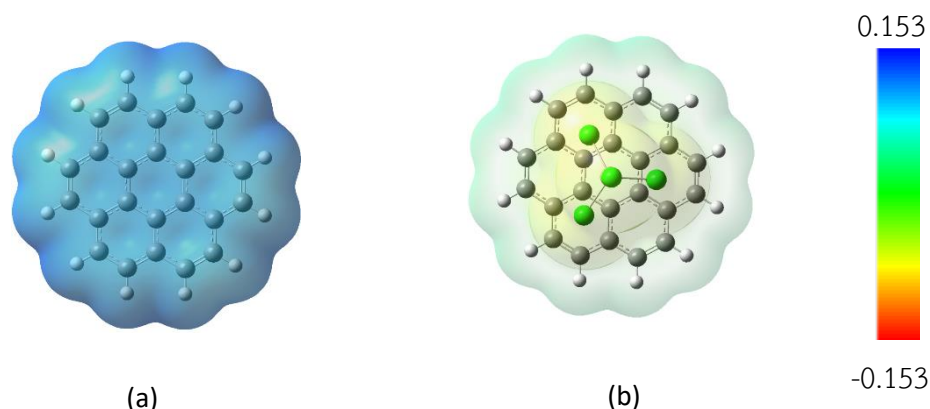
0.153

-0.153

Figure 4.2. Electrostatic potential of coronene (a), [AlCl$_4$]-coronene
(b) in charging condition.

4.1.2 Discharging condition

For discharging condition, the reaction is reversed from the charging one. In this case, the C$_n$ charge is neutral while AlCl$_4$ is -1. Therefore, the charge of coronene was set to 0 in the discharging condition.

4.1.2.1 Adsorption energy in discharging condition

Adsorption energies for [AlCl$_4$]$^-$ on coronene in discharging condition were listed in Table 4.3. Adsorption energies between -0.53 and -5.31 kcal/mol were observed for all adsorption patterns. Thus, they are all weak. The strongest adsorption for [AlCl$_4$]-coronene was noticed for T2-III with the adsorption energy of -5.31 kcal/mol. However, this value is only 0.15 kcal/mol below the B4-III adsorption. The H1-I was the weakest adsorption, its value was probably less than BSSE implying no adsorption.

Table 4.3. Possible adsorptions, adsorption energies, voltage and

Mulliken charges of [AlCl$_4$]-coronene in discharging condition

Adsorption Pattern	E$_{ads}$ (kcal/mol)	C-Cl distance	Mulliken Charge of AlCl$_4^-$	Mulliken Charge of GQDs
H1-I	-0.53	3.22	-1.06	0.00
H1-II	-2.22	3.35	-1.02	0.00
H1-III	-3.82	3.36	-0.95	-0.05
H2-II	-1.81	3.40	-1.01	0.00
B4-III	-5.16	3.21	-0.93	-0.07
T2-III	-5.31	3.22	-0.92	-0.08
T1-III	-4.02	3.37	-0.94	-0.06

4.1.2.2 Charge transfer in discharging condition

Net charges of [AlCl$_4$]$^-$ after adsorption on coronene surface in discharging condition were shown in Table 4.3. The charge of [AlCl$_4$]$^-$ after adsorption in this condition do not change significantly from -1. Therefore, in discharging condition, there are small amount of charge being transferred from [AlCl$_4$]$^-$ to coronene surface. The charge transfer of [AlCl$_4$]$^-$ to coronene can be best viewed from electrostatic potential map in Figure 4.3. From the figure, the coronene charge change from small negative to large negative after the adsorption.
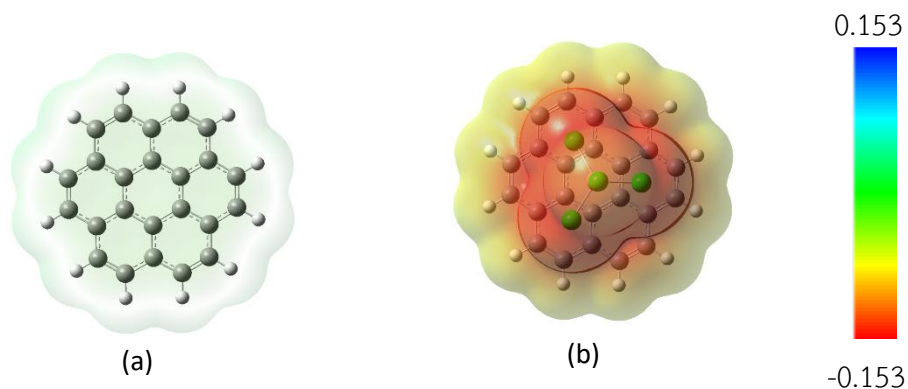
Figure 4.3. Electrostatic potential of coronene (a), [AlCl$_4$]-coronene

(b) in discharging condition.

4.2 ADSORPTION ON CIRCUMCORONENE

Adsorbed sites and standing positions of [AlCl$_4$]$^-$ on circumcoronene after optimization were shown in Table 4.4. Only the standing position III were considered in this case. Since from the previous section we found the standing position III to be the most stable position. Based on Table 4.4. we can see that in central area, [AlCl$_4$]$^-$ prefers to be adsorbed on hollow and on-top site while in edge area it prefers to be adsorbed on bridge and on-top site.

Table 4.4. Optimized structures of [AlCl$_4$]-circumcoronene
in discharging and charging condition.

Sites and Standing	After optimization on discharging condition	After optimization on charging condition
	III	III
B1	T1-III	T1-III
B2	H2-III	T2-III
B3	T3-III	T3-III
B4	B4-III	B4-III
B5	B4-III	B4-III
H1	H1-III	H1-III
H2	H2-III	H2-III
H3	B4-III	T2-III
H4	B4-III	T2-III
T1	T1-III	T1-III
T2	T2-III	T2-III
T3	T3-III	T3-III
T4	T4-III	B4-III

4.2.1 Charging Condition

4.2.1.1 Adsorption energy in charging condition

Adsorption energies for [AlCl$_4$] and circumcoronene in charging condition was listed in Table 4.5. The values between -54.26 and -57.01 kcal/mol were observed. The strongest adsorption is noticed for T1-III with the adsorption energy of -57.01 kcal/mol. This is little bit weaker than the case of coronene. The C-Cl distance between [AlCl$_4$] and circumcoronene agree well with previous report [12-14] with values between 3.08 and 3.33 Å.

Table 4.5. Possible adsorptions, adsorption energies, voltage and Mulliken charges of [AlCl$_4$]-circumcoronene in charging condition

Adsorption Site	E$_{ads}$ (kcal/mol)	C-Cl distance	Mulliken Charge of AlCl$_4^-$	Mulliken Charge of GQDs
H1-III	-56.52	3.27	-0.90	0.90
H2-III	-56.41	3.30	-0.88	0.88
B2-III	-56.10	3.33	-0.88	0.88
B4-III	-56.34	3.20	-0.83	0.83
T1-III	-57.01	3.27	-0.89	0.89
T2-III	-56.45	3.08	-0.88	0.88
T3-III	-54.26	3.08	-0.83	0.83
T4-III	-56.33	3.23	-0.83	0.83

4.2.1.2 Charge transfer in charging condition

The molecular charge for $[AlCl_4]^-$ is -1. Net charges of $[AlCl_4]^-$ after adsorption on circumcoronene surface in charging condition were shown in Table 4.5. From the results, the charges are in the range of -0.83 to -0.90. These values are higher than the charge of $[AlCl_4]^-$. This is little bit lower than the case of coronene. Therefore, in the charging condition, there is the charge transfer from $[AlCl_4]^-$ to circumcoronene surface. We also can view the nature of the interaction between $[AlCl_4]^-$ and GQDs from electrostatic potential map in Figure 4.4. Circumcoronene is less positive compare than coronene based on the electrostatic potential.
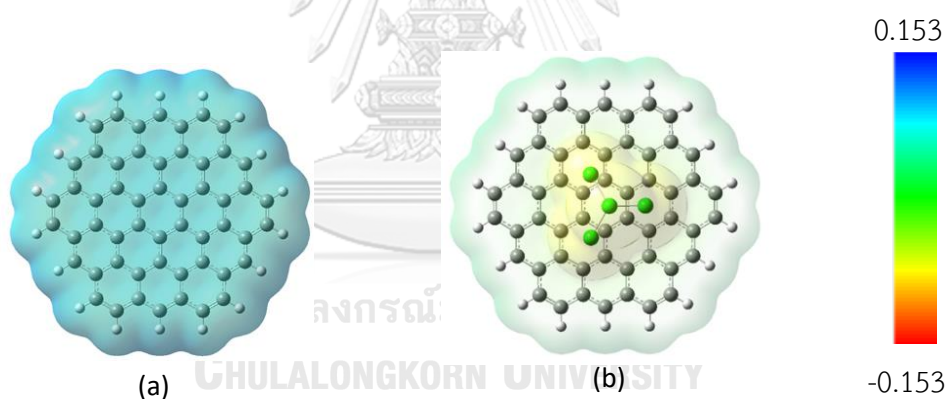

(a)   (b)

0.153

-0.153

Figure 4.4. Electrostatic potential of circumcoronene (a),
$[AlCl_4]$-circumcoronene (b) in charge condition.

4.2.2 Discharging condition

4.2.2.1 Adsorption energy in discharging condition

Adsorption energies for [AlCl$_4$]$^-$ and circumcoronene in discharging condition were listed in Table 4.6. Adsorption energies between -6.78 and -8.81 kcal/mol were observed for [AlCl$_4$]-circumcoronene, a stronger binding a those of coronene in the discharging condition. However, all adsorptions are still considered as weak. The strongest adsorption for [AlCl$_4$]-circumcoronene was noticed for B4-III with the adsorption energy of -8.81 kcal/mol. However, this value is only 0.41 kcal/mol below the T3-III adsorption.

Table 4.6. Possible adsorptions, adsorption energies, voltage and Mulliken charges of [AlCl$_4$]-circumcoronene in discharging condition

Adsorption Site	E$_{ads}$ (kcal/mol)	C-Cl distance	Mulliken Charge of AlCl$_4^-$	Mulliken Charge of GQDs
H1-III	-7.06	3.31	-0.96	-0.04
H2-III	-7.03	3.33	-0.94	-0.06
B4-III	-8.81	3.16	-0.90	-0.10
T1-III	-6.89	3.31	-0.92	-0.08
T2-III	-6.78	3.33	-0.92	-0.08
T3-III	-8.40	3.25	-0.90	-0.10
T4-III	-8.29	3.20	-0.91	-0.09

4.2.2.2 Charge transfer in discharging condition

Net charges of $[AlCl_4]^-$ after adsorption on circumcoronene surface in discharging condition were shown in table 4.6. The charge of $[AlCl_4]^-$ after adsorption in this condition does not change significantly compared with the charge of $[AlCl_4]^-$. Mostly these values remain unaltered from the charge of $[AlCl_4]^-$. Therefore, in discharging condition, the charge transfer from $[AlCl_4]^-$ to circumcoronene surface is very small. We also can view the nature of the interaction between $[AlCl_4]^-$ and GQDs from electrostatic potential map in Figure 4.5.
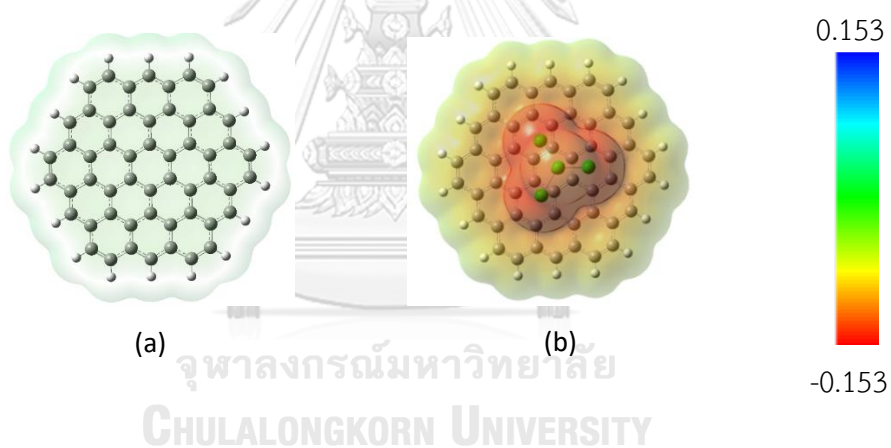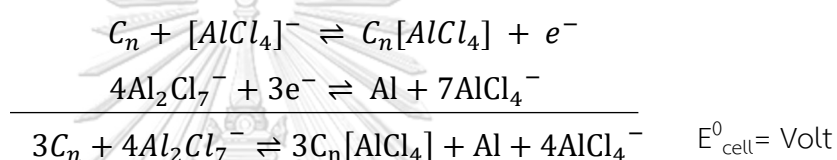

Figure 4.5. Electrostatic potential of circumcoronene (a),
$[AlCl_4]$-circumcoronene (b) in discharging condition.

4.3 ELECTROCHEMICAL PROPERTIES OF [AlCl$_4$]$^-$ ADSORBED ON GQDs

Adsorption of [AlCl$_4$]$^-$ on GQDs surface is the important thing in the mechanism of ultrafast rechargeable aluminum battery which already discussed in section 2.2. Adsorption mechanism affected the electrochemical process of the battery. One of the electrochemical properties is the voltage. The theoretical voltage of Aluminum-ion battery using [AlCl$_4$]-coronene and [AlCl$_4$]-circumcoronene as cathode can be determined using the following reaction;

$$C_n + [AlCl_4]^- \rightleftharpoons C_n[AlCl_4] + e^-$$
$$\underline{4Al_2Cl_7{}^- + 3e^- \rightleftharpoons Al + 7AlCl_4{}^-}$$
$$3C_n + 4Al_2Cl_7{}^- \rightleftharpoons 3C_n[AlCl_4] + Al + 4AlCl_4{}^- \qquad E^0{}_{cell} = Volt$$

Using the equation 3.2, theoretical voltage of [AlCl$_4$]-GQDs can be obtained by

$$V = \left(\frac{\left\{ 3E_{[AlCl_4]Cn} + 4E_{[AlCl_4{}^-]} + E_{Al} \right\} - \left\{ 3E_{Cn} + 4E_{[Al_2Cl_7{}^-]} \right\}}{nF} \right)$$

Where n is the number of transferred electron during redox reaction, F is the faraday constant (23.061 kcal per volt gram), and E is the energy of each species (kcal/mol). Values of theoretical voltage was given in Table 4.7. for [AlCl$_4$]-coronene and Table 4.8. for [AlCl$_4$]-circumcoronene.

Table 4.7. Theoretical Voltage of [AlCl$_4$]-coronene

Adsorption Site	Adsorption E (kcal/mol)	Total E (kcal/mol)	Ecell (V)
H1-III	-65.24	-299.72	-4.33
B1-III	-64.08	-296.23	-4.28
B2-III	-64.07	-296.19	-4.28
B4-III	-63.20	-293.59	-4.24
T1-III	-64.05	-296.15	-4.28
T3-III	-63.03	-293.07	-4.24

Table 4.8. Theoretical Voltage of [AlCl$_4$]-circumcoronene

Adsorption Site	Adsorption E (kcal/mol)	Total E (kcal/mol)	Ecell (V)
H1-III	-56.52	-273.56	-3.95
H2-III	-56.41	-273.21	-3.95
B2-III	-56.10	-272.31	-3.94
B4-III	-56.34	-273.02	-3.95
T1-III	-57.01	-275.03	-3.98
T2-III	-56.45	-273.35	-3.95
T3-III	-54.26	-266.77	-3.86
T4-III	-56.33	-272.99	-3.95

In the introduction chapter, we mention that the objective of this work is to increase the voltage of aluminum battery (1.7 V) [1-2]. Lin [3] achieved the voltage of rechargeable aluminum battery of 2.45 V. Several computational studies also report their works; Gao [13] mentioned the charging potential profile of rechargeable aluminum battery of 2.06 V. Using similar methods, Bhauriyal [14] reported their

results in range 1.58 V to 3.91 V. Our results showed that the voltage is linear to the

adsorption energy and can be as high as -4.33 V for coronene. Its means that the

structure which has high adsorption energy also will have high theoretical voltage.

4.4 DESIGNING CATHODE MATERIAL

Our result showed that $[AlCl_4]^-$ adsorbed on all possible adsorption sites of GQDs

such as bridge, hollow and on-top. It means that GQDs is an active adsorbent. The

value of adsorption energy in charging condition is high means that GQDs and $[AlCl_4]^-$

has strong interaction. While in discharging condition the adsorption is weak. Thus, in

this condition $[AlCl_4]^-$ can easily be released from GQDs. On the other hand, GQDs

can strongly adsorbed $[AlCl_4]^-$ in the charging condition. Therefore, GQDs is the

suitable materials for use as cathode in Aluminum-ion battery.

CHAPTER 5

CONCLUSION

DFT calculations using M06-2X methods with 6-31G+(d) basis set were employed to determine the optimized structure and the adsorption energy of $[AlCl_4]$-GQDs respectively. Two hexagonal shapes of GQDs, coronene ($C_{24}H_{12}$) and circumcoronene ($C_{54}H_{18}$) used as models of cathode materials. These results revealed that $[AlCl_4]^-$ adsorbed on several types of site such as bridge, hollow and on-top sites. Hollow and on-top sites are the preferable adsorption site in central area while bridge and on-top site in edge area. The result also showed that the structure of $[AlCl_4]^-$ with position III is the most favourable position. The adsorption energy expressed about the most stable structure of $[AlCl_4]$-GQDs. Based on the result, the highest adsorption energy in discharging condition is T2-III (edge) for $[AlCl_4]$-coronene and T4-III (edge) for $[AlCl_4]$-circumcoronene. The theoretical voltage is important to predict the performance of the $[AlCl_4]$-GQDs battery. From the result, GQDs cathode material increased the voltage of aluminum battery (3.27-3.66 V) which is higher than previous aluminum battery (1.7 V). Our results concluded that the aluminum battery with GQDs cathode material can be recommended as a new sophisticated battery.

REFERENCES

1. Elia, G.A., et al., *An overview and future perspectives of aluminum batteries.* Advanced Materials, 2016. **28**(35): p. 7564-7579.

2. Zafar, Z.A., et al., *Cathode materials for rechargeable aluminum batteries: current status and progress.* Journal of Materials Chemistry A, 2017. **5**(12): p. 5646-5660.

3. Lin, M.-C., et al., *An ultrafast rechargeable aluminium-ion battery.* Nature, 2015. **520**(7547): p. 324.

4. Li, Q. and N.J. Bjerrum, *Aluminum as anode for energy storage and conversion: a review.* Journal of Power Sources, 2002. **110**(1): p. 1-10.

5. Jayaprakash, N., S. Das, and L. Archer, *The rechargeable aluminum-ion battery.* Chemical Communications, 2011. **47**(47): p. 12610-12612.

6. Wang, W., et al., *A new cathode material for super-valent battery based on aluminium ion intercalation and deintercalation.* Scientific reports, 2013. **3**: p. 3383.

7. Gifford, P. and J. Palmisano, *A substituted imidazolium chloroaluminate molten salt possessing an increased electrochemical window.* Journal of the Electrochemical Society, 1987. **134**(3): p. 610-614.

8. Sun, H., et al., *A new aluminium-ion battery with high voltage, high safety and low cost.* Chemical Communications, 2015. **51**(59): p. 11892-11895.

9. Hudak, N.S., *Chloroaluminate-doped conducting polymers as positive electrodes in rechargeable aluminum batteries.* The Journal of Physical Chemistry C, 2014. **118**(10): p. 5203-5215.

10. Geng, L., et al., *Reversible electrochemical intercalation of aluminum in Mo6S8.* Chemistry of Materials, 2015. **27**(14): p. 4926-4929.

11. Wu, M., et al., *Geometry and fast diffusion of AlCl4 cluster intercalated in graphite.* Electrochimica Acta, 2016. **195**: p. 158-165.

12. Jung, S.C., et al., *Flexible few-layered graphene for the ultrafast rechargeable aluminum-ion battery.* The Journal of Physical Chemistry C, 2016. **120**(25): p. 13384-13389.

13.   Gao, Y., et al., *Understanding ultrafast rechargeable aluminum-ion battery from first-principles.* The Journal of Physical Chemistry C, 2017. **121**(13): p. 7131-7138.

14.   Bhauriyal, P., A. Mahata, and B. Pathak, *The staging mechanism of AlCl 4 intercalation in a graphite electrode for an aluminium-ion battery.* Physical Chemistry Chemical Physics, 2017. **19**(11): p. 7980-7989.

15.   Zhu, C., et al., *Enhanced lithium storage performance of CuO nanowires by coating of graphene quantum dots.* Advanced Materials Interfaces, 2015. **2**(2): p. 1400499.

16.   Chao, D., et al., *Graphene quantum dots coated VO2 arrays for highly durable electrodes for Li and Na ion batteries.* Nano letters, 2014. **15**(1): p. 565-573.

17.   Chen, W., et al., *Synthesis and applications of graphene quantum dots: A review.* Nanotechnology Reviews, 2018. **7**(2): p. 157-185.

18.   Jegannathan, P., et al., *Enhancement of graphene quantum dots based applications via optimum physical chemistry: A review.* Biocybernetics and Biomedical Engineering, 2018. **38**(3): p. 481-497.

19.   Jin, Z., et al., *Graphene, graphene quantum dots and their applications in optoelectronics.* Current opinion in colloid & interface science, 2015. **20**(5-6): p. 439-453.

20.   Bak, S., D. Kim, and H. Lee, *Graphene quantum dots and their possible energy applications: A review.* Current Applied Physics, 2016. **16**(9): p. 1192-1201.

21.   Zeng, Z., et al., *Graphene quantum dots (GQDs) and its derivatives for multifarious photocatalysis and photoelectrocatalysis.* Catalysis Today, 2018. **315**: p. 171-183.

22.   Guo, J., et al., *Boosting the lithium storage performance of MoS 2 with graphene quantum dots.* Journal of Materials Chemistry A, 2016. **4**(13): p. 4783-4789.

23.   Sadlej-Sosnowska, N., *Ab Initio Study of Charge Transfer between Lithium and Aromatic Hydrocarbons. Can the Results Be Directly Transferred to the*

Lithium–Graphene Interaction? The Journal of Physical Chemistry A, 2014. **118**(34): p. 7044-7051.

24. Ruzanov, A., et al., *Density Functional Theory Study of Ionic Liquid Adsorption on Circumcoronene Shaped Graphene.* The Journal of Physical Chemistry C, 2018. **122**(5): p. 2624-2631.

25. Thinius, S., et al., *Theoretical study of Li migration in lithium–graphite intercalation compounds with dispersion-corrected DFT methods.* The Journal of Physical Chemistry C, 2014. **118**(5): p. 2273-2280.

26. Levine, I. N., *Quantum chemistry, Seventh Edition,.* 2014. Pearson Education. ISBN-13: 978-0-321-80345-0.

27. Born, M. and R. Oppenheimer, *Zur quantentheorie der molekeln.* Annalen der physik, 1927. **389**(20): p. 457-484.

28. Cramer. C.J., *Essentials of Computational Chemistry: Theories and Models, Second Edition*. 2004. John Wiley & Sons.

29. Jansen, F., *Introduction to Computational Chemistry, Third Edition.* 2017 John Wiley & Sons. ISBN 9781118825983.

30. Roothaan, C.C.J., *New developments in molecular orbital theory.* Reviews of modern physics, 1951. **23**(2): p. 69.

31. Hall, G.G., *The molecular orbital theory of chemical valency VIII. A method of calculating ionization potentials.* Proceedings of the Royal Society of London. Series A. Mathematical and Physical Sciences, 1951. **205**(1083): p. 541-552.

32. March, N.H. and S. Lundqvist, *Theory of the inhomogeneous electron gas*. 1983: Plenum Press.

33. Cramer, C.J. and D.G. Truhlar, *Density functional theory for transition metals and transition metal chemistry.* Physical Chemistry Chemical Physics, 2009. **11**(46): p. 10757-10816.

34. Deutschmann, O., F. Behrendt, and J. Warnatz, *Modelling and simulation of heterogeneous oxidation of methane on a platinum foil.* Catalysis Today, 1994. **21**(2-3): p. 461-470.

35. Slater, J.C., *The theory of complex spectra.* Physical Review, 1929. **34**(10): p. 1293.

36.   Schlegel, H.B. and M.J. Frisch, *Transformation between Cartesian and pure spherical harmonic Gaussians.* International Journal of Quantum Chemistry, 1995. **54**(2): p. 83-87.

37.   Young, D., 2004. Computational chemistry: a practical guide for applying techniques to real world problems. John Wiley & Sons.

38.   Dunning Jr, T.H., 1989. Gaussian basis sets for use in correlated molecular calculations. I. The atoms boron through neon and hydrogen. The Journal of chemical physics, 90(2), pp.1007-1023.

39.   Zhao, Y. and Truhlar, D.G., 2008. The M06 suite of density functionals for main group thermochemistry, thermochemical kinetics, noncovalent interactions, excited states, and transition elements: two new functionals and systematic testing of four M06-class functionals and 12 other functionals. Theoretical Chemistry Accounts, 120(1-3), pp.215-241.

40.   Alonso-Lanza, T., Mañanes, A. and Ayuela, A., 2017. Interaction of cobalt atoms, dimers, and Co4 clusters with circumcoronene: A theoretical study. The Journal of Physical Chemistry C, 121(34), pp.18900-18908.
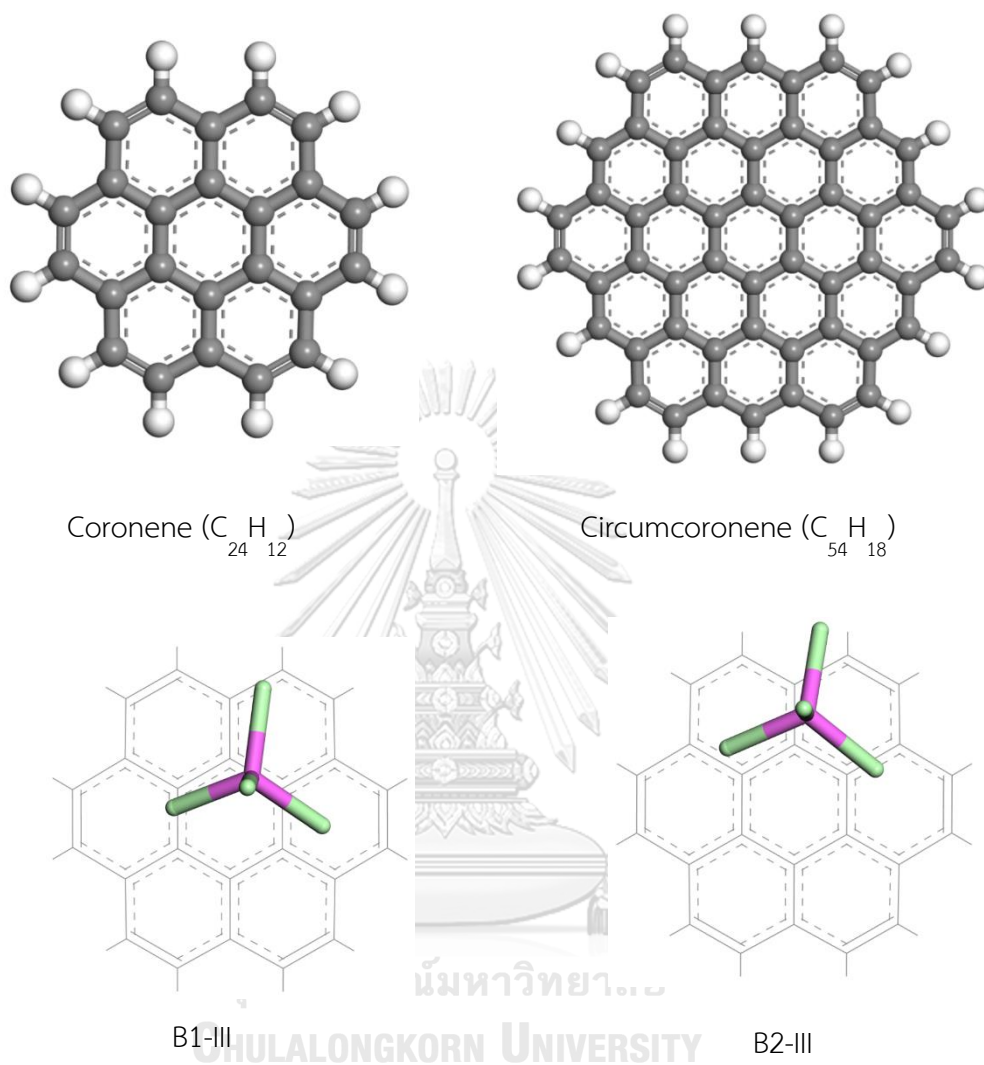
APPENDIX

Coronene ($C_{24}H_{12}$)

Circumcoronene ($C_{54}H_{18}$)

B1-III

B2-III

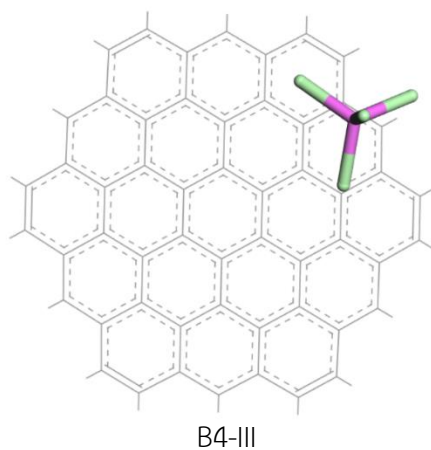**Figure A-1** The M06-2X/6-31G+(d) optimized geometries of GQDs.

B4-III

Figure A-2 The M06-2X/6-31G+(d) optimized geometries of [AlCl$_4$]-GQDs at bridge position.
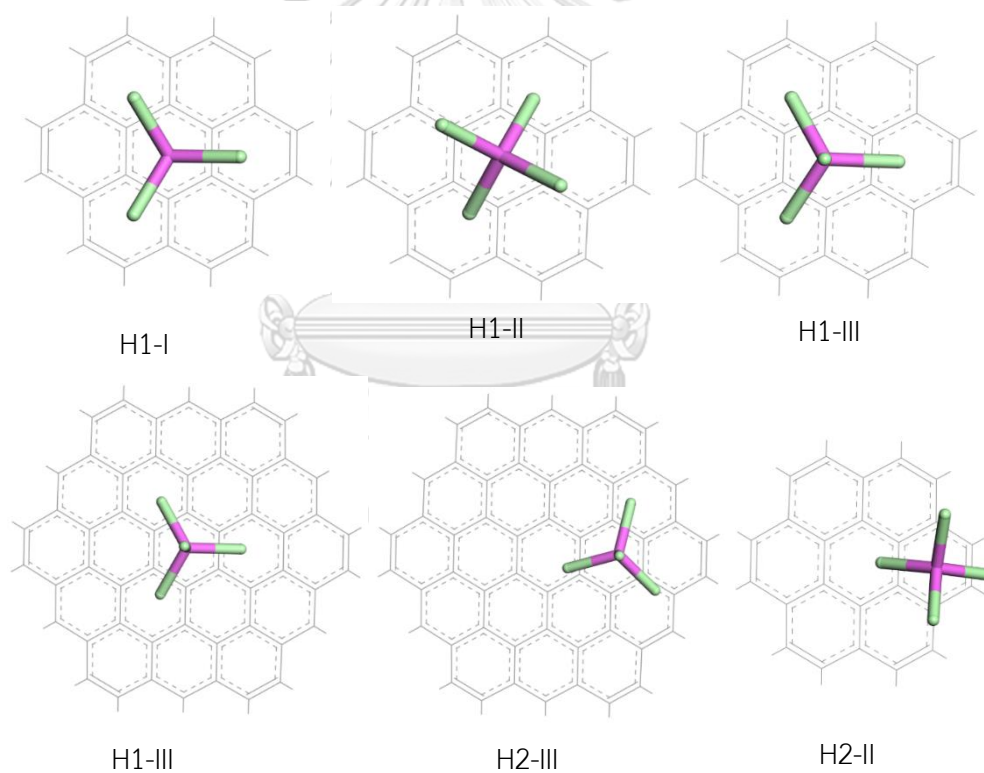

H1-I

H1-II

H1-III

H1-III

H2-III

H2-II

Figure A-3 The M06-2X/6-31G+(d) optimized geometries of [AlCl$_4$]-GQDs at hollow position.

T1-III T2-III T3-III

T1-III T2-III

T3-III T4-III
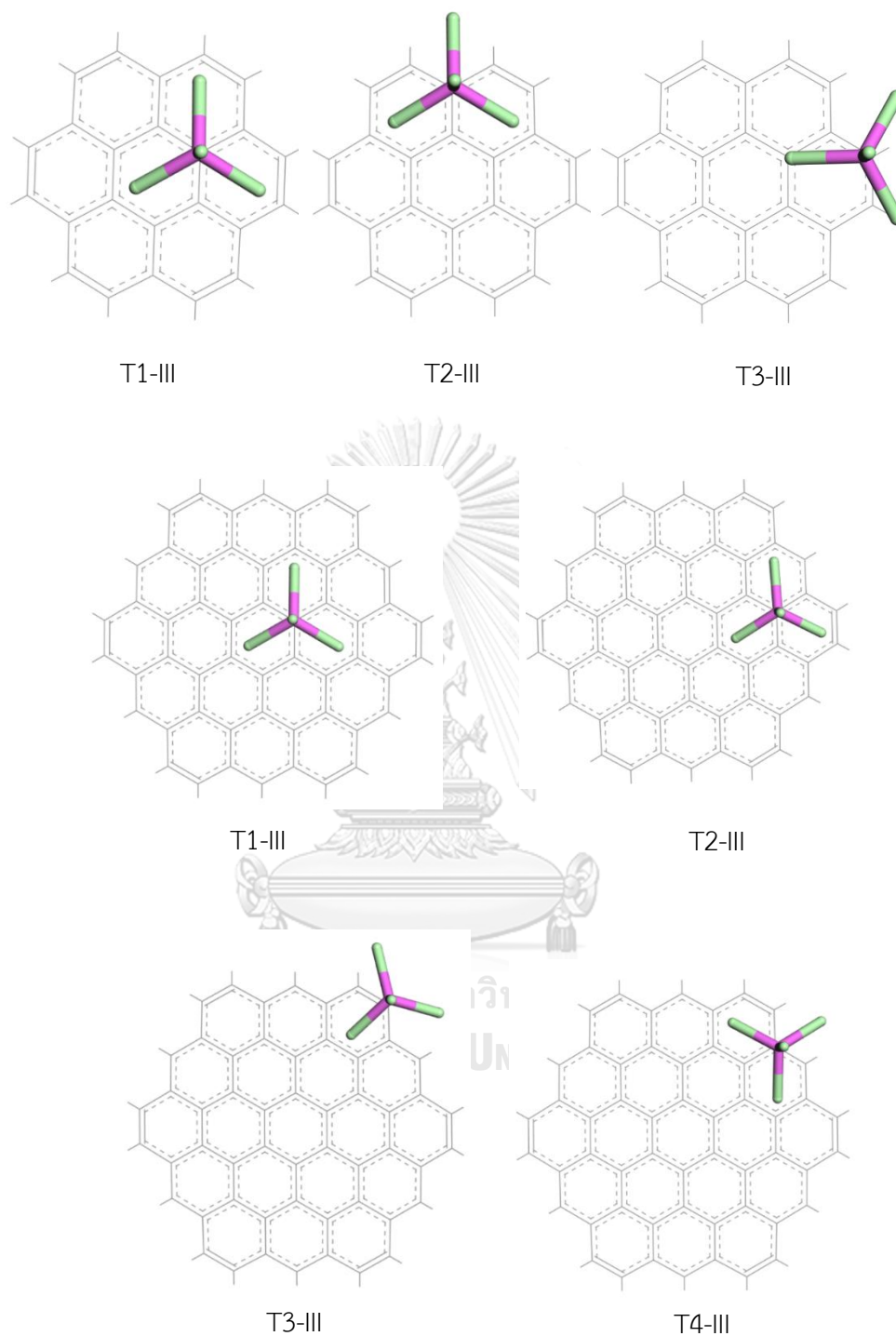
Figure A-4 The M06-2X/6-31G+(d) optimized geometries of

[AlCl$_4$]-GQDs at on-top position.

H1-III   B1-III   B2-III

B4-III   T1-III   T3-III
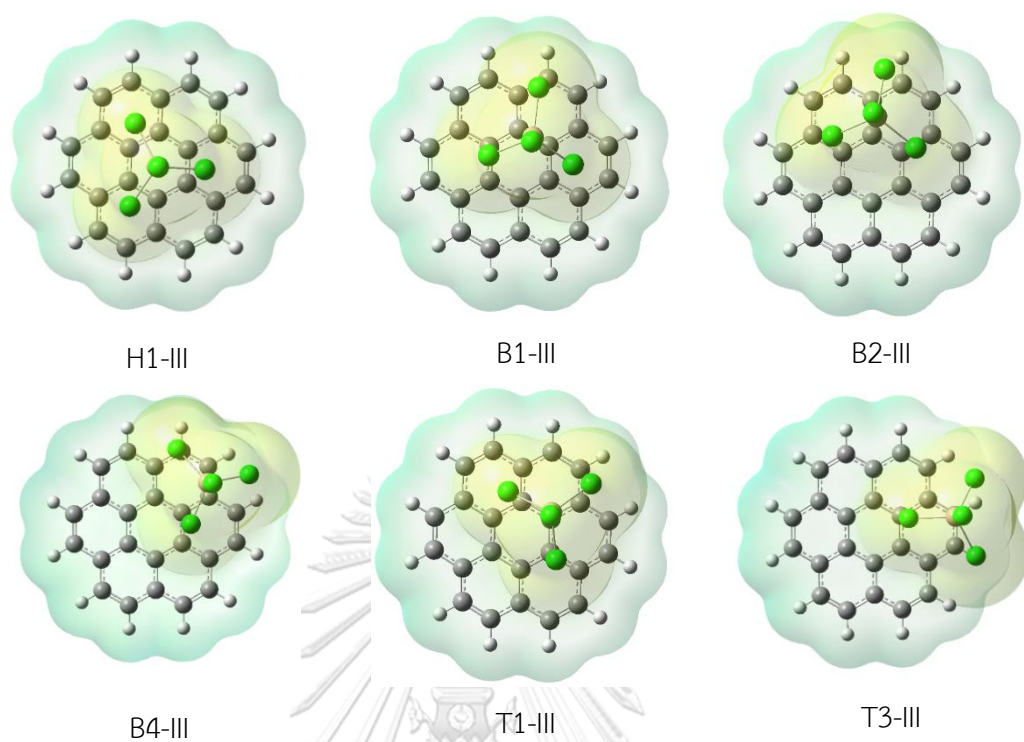
Figure A-5 Electrostatic potential of [AlCl$_4$]-coronene in charging condition

H1-1

H2-II

HI-III

T1-III

T2-III

B4-III
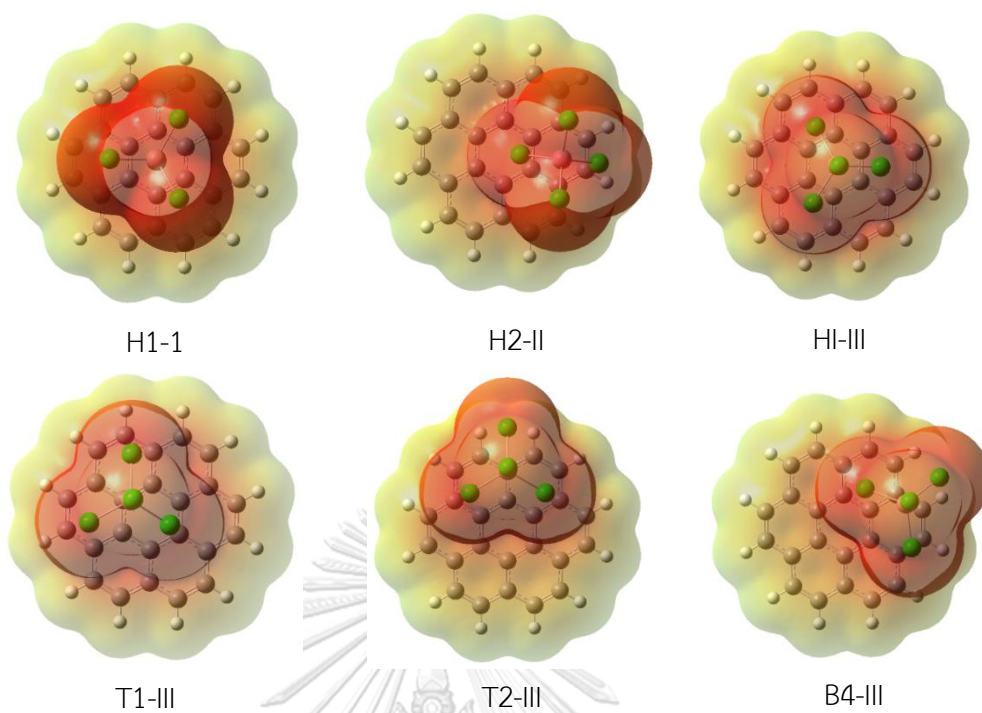
Figure A-6 Electrostatic potential of [AlCl$_4$]-coronene in discharging condition

H1-III

B4-III

B2-III

T1-III

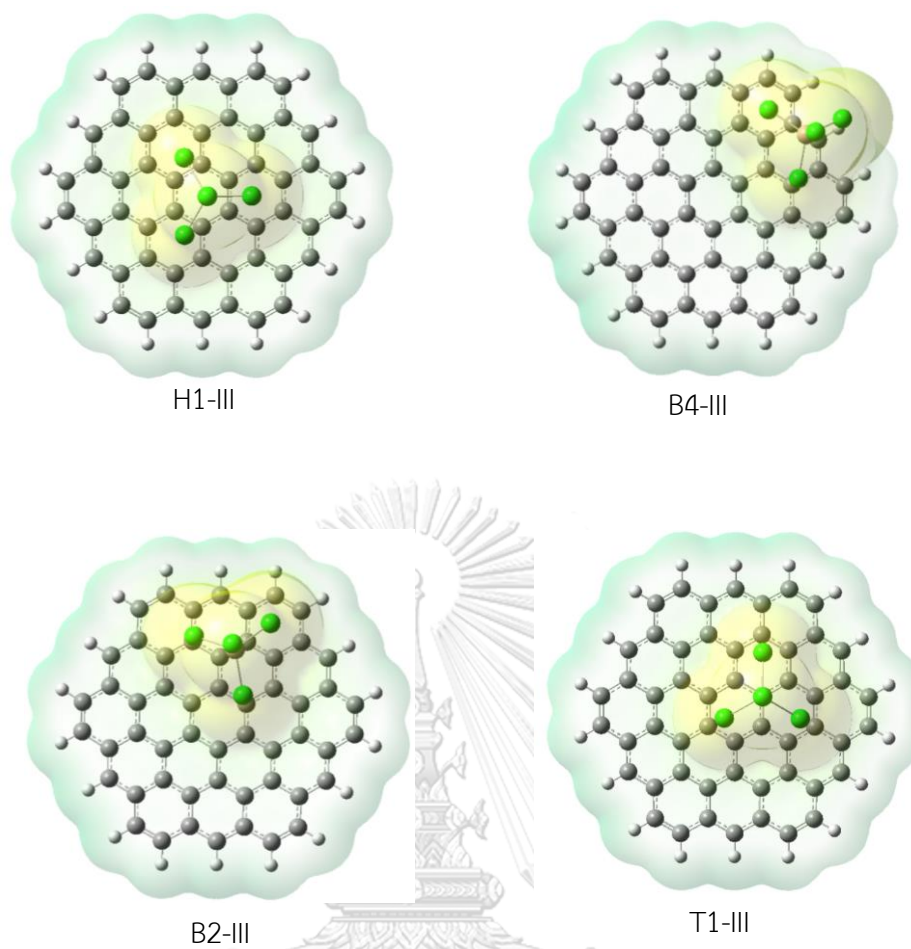**Figure A-7** Electrostatic potential of [AlCl$_4$]-circumcoronene in charging condition
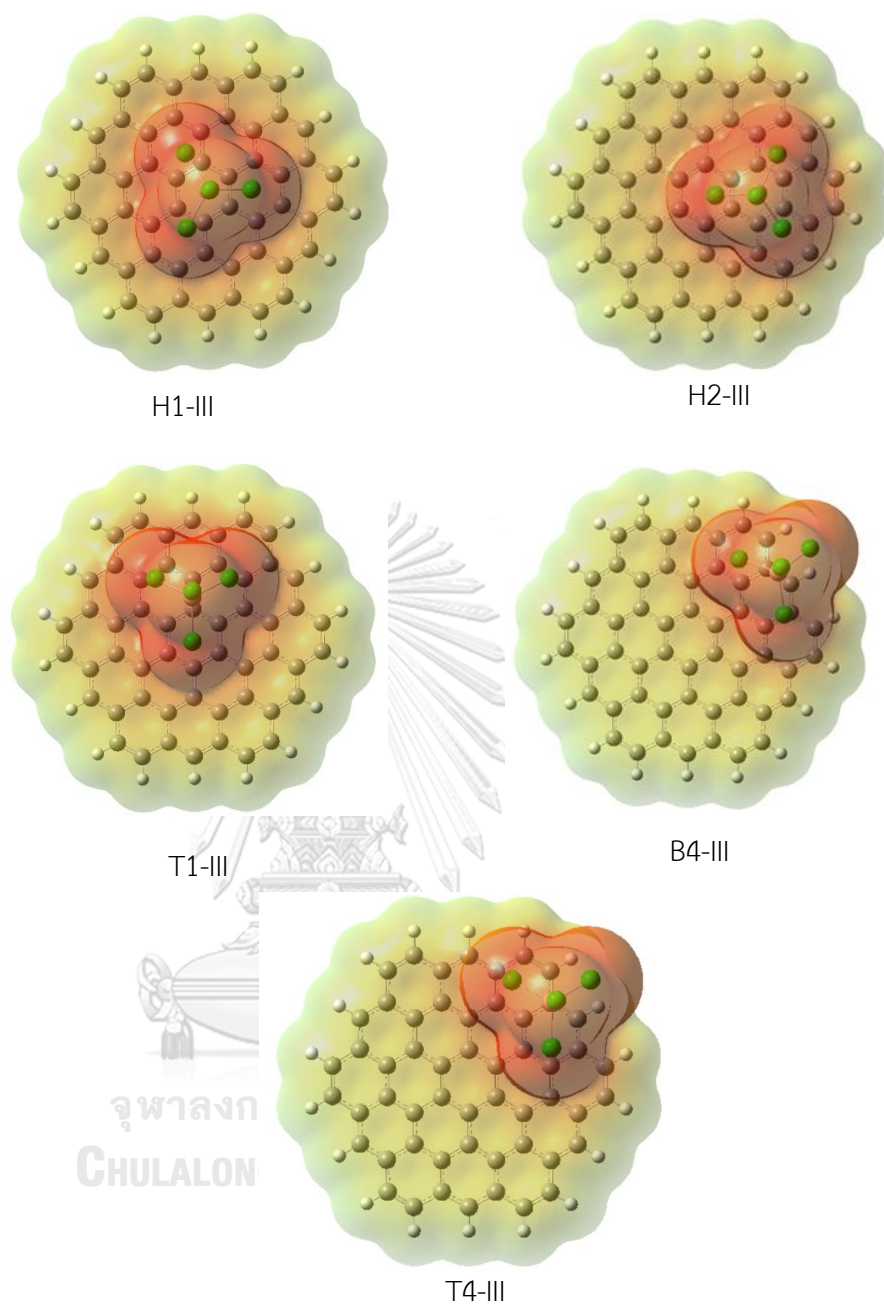
Figure A-8 Electrostatic potential of [AlCl$_4$]-circumcoronene

in discharging condition

VITA

NAME   Fadjar Mulya

DATE OF BIRTH   06 September 1993

PLACE OF BIRTH   Jambi, Indonesia

INSTITUTIONS ATTENDED   Chemistry Department, Faculty of Science, Chulalongkorn
                        University

HOME ADDRESS   Ngampilan NG I/179, Yogyakarta, Indonesia